Matter

Article

Matter

Article

The Rashba Scale: Emergence of Band Anti-crossing as a Design Principle for Materials with Large Rashba Coefficient

Carlos Mera Acosta,[1,2] Elton Ogoshi,[2] Adalberto Fazzio,[3] Gustavo M. Dalpian,[2] and Alex Zunger[1,4,*]

SUMMARY

The spin-orbit-induced spin splitting of energy bands in low-symmetry compounds (the Rashba effect) has a long-standing relevance to spintronic applications and the fundamental understanding of symmetry breaking in solids, yet the knowledge of what controls its magnitude in different materials is ext

agnetic eld that leads to spin-split and polarized bands. The magnitude of t

' is given by the ratio between the spin splitting E

k_R, a , _R = 2E_R/k_R. S ; a a Ra a a a a

a (DFT)- a a a Ra a . S -

, a Ra a a a a

W a a a, Ra a -

a a a ; a 1 V ; a a a
a . T ; a a a ; a
Ra a a a a a a a a -
a . W (" Ra a ,"[13] -
a R-1). W (1) a; (-

a SOC (. ., a_R = 2at

a . ; a . a - ; a
. (F ; 1).

W F ; 5 DFT- a a . a . a a . a - . a .
. F ; 1 ; Ra a . . F a , B T I (F ; 5A),
k<k_R, T -sp_z (T -p_{xy}) a VBM (a .
[CBM]), k<k_R, a CBM (VBM), a . a . -
a; a (;) . a . . T . a a . a - ; . A

-a , a a a a a (S -
a l a III). T TI a a a [25 27] a 0, 0, a 3
- a TRI , : S 2T S 2, $K_5F_2O_6$, a T N.
U a , a DFT a a a , $K_5F_2O_6$
a a a (E_{AFM} □ E_{FM} = 2.7 V

a , a Ra a a a a-
. I , a a (a ; a a NC a ; ,
a Ta 1) a a
Ra a . T ; ; a a TRI a
; Ra a , a Ra a
a a a ; a a - ; .

Discovery of Strong Rashba Compounds via DFT Prediction of Band Anti-crossing

T ; - a TI a a a
Ra a , a ; TI a ; a a Ra a .
T a a , ; a , a Ra a a
a a a - ; a a TI . I
a a a a a a ; a a -
a .

A a Ra a , a a a
Ra a a ; : ;
a a , a , a
a . F a , a F ; 2A KS $_2$S $_4$, a
a a Γ_{1v} a Γ^0_{1v} a ; Γ-X a a
a , a ; a ; Ra a a a . H ,
a - ; a a a , Ra a a
a a ; a . H , a a a a ;
a ; Ra a ; , . ., a VBM CBM. T
a - ; a ; a .

F ; 8 a ; a ; , ,
; , a F ; 8. S -
a I a III a a a ; .
W a a a a Ra a R-1 , . .,

a a a

(F, 3

Ra a a a RSS a ; . O a , -
a ; a a RSS a k- , . .,
VBM a CBM. T a (a) RSS a
- a (Ta 2) a ( )
RSS a a ; (Ta 3 a 4). I ; , RSS
a VBM CBM; a a a
KS S ($P6_3mc$) RSS 80 V a Ra a a a 3.86 VA
CBM.

Conclusion

a a - a
a a a Ra a .

EXPERIMENTAL PROCEDURES

Density Functional Theory Calculations

T DFT a a a ; P -B -E - ; a ; a a a (PBE)[62] a ; - a a a H a - [63,64] a V a A - S a- Pa a; .[65,66] W a AFLOW- a a- a [59] a ; a; ; a a a; a - a; a ; a ; a ICSD.[43] O a a a ; a - a; - ; a C a a .[59] a - a; . T a a - - a; a , a C a a .[59] a a a; a a a ; a a; a (a FM) a a ; - a ; a . A ; a a SOC(.; ., ; , k- a ; , U a a -) a a a C a a .[59]

High-Throughput DFT Quantification of Rashba Coefficients

F a RSS, α_R ; a ; ; a - , . ., $\alpha_R = 2E_R/k_R$. H , a Ra a a B .[20] T a a , a a - ; a , a k- . H , Ra a a VBM a CBM a a a ; ; - k- . A a

a a a a a k , p (.; ., Ha -
a E a 1) ; L , S (. ., Ra a k_R $_y k_x$ - -
a), a .

F $k \to 0$, ; a $t_{pp} = t_{pp}^{\uparrow\uparrow} = t_{pp}^{\downarrow\downarrow}$, Ha a a -
p- a a , a ,

$H_p(k) = \varepsilon_p + 2t_{pp} - t_{pp} a^2 k_x^2 - i2t^p k_x a$

a , a a . 1D a
a .

N a . s- a a a a a a ; a -
a J = 1/2, a . . . .
a a . . p_z- a , a. a - SOC. T s- -
a . a RSS, SOC . I a , a . Ha -
a Hðkþ a a . . A a a . Fa [12] a -
a a a ; a J = 1/2 a . J = 3/2.

Resource Availability

Lead Contact

A ∠ ; . E a a . . : a . ; @ a . . .

Materials Availability

T . ⌐ . . ; a a; .

Data and Software Availability

A . a a . . a a a a a a
a . S a l a . A . a . a a a . a a ⌐ -
. a .

SUPPLEMENTAL INFORMATION

Ma e , V . l e 3

S d e a l a

T e Ra ba Sca d: E e ce

Ba d A -c a a De P c d

Ma e a l N La e Ra ba C e fic e

Carlos Mera Acosta, Elton Ogoshi, Adalberto Fazzio, Gustavo M. Dalpian, and Alex Zunger

The Rashba Scale: Emergence of Band Anti-Crossing as a Design Principle for Materials with Large Rashba coefficient

1 Weak Rashba compounds

Table S1 - Weak Rashba materials with spin splitting in both VBM and CBM. For each compound we present the ICSD code, space group, high symmetry *k*-point for the Rashba splitting in the valence (K_V

$BiKP_2Se_6$	4	90153	X	12.7	0.08	0.318	Y	47.1	0.108	0.873
KP_2SbSe_6	4	90152	X	18.7	0.08	0.467	Y	60.6	0.14	0.864
$Bi_4Br_2O_9Te_2$	99	79508	Z	3.6	0.014	0.51	G	5.4	0.014	0.757
$HfNO_3Ta$	4	186409	X	33.4	0.168	0.397	X	8.3	0.032	0.516
$HO_{10}P_3Pb_2$	1	2494	R	1.2	0.049	0.047	X	11	0.051	0.433
F_4HKOTe	4	155199	E	8.3	0.127	0.131	Y	4.2	0.021	0.395
$AgBiCr_4O_{14}$	79	14234	M	4	0.066	0.121	G	27.5	0.205	0.268
$AsCu_4KS_4$	4	75430	G	8.5	0.05	0.339	Y	2.8	0.025	0.224
AuC_2ClH_3N	4	152108	X	1.9	0.073	0.052	Y	1.6	0.018	0.177

Table S2 - Weak Rashba materials with spin splitting in the CBM. For each compound we present the ICSD code, space group, high symmetry *k*-point for the Rashba splitting in the conduction bands (K_c), Rashba spin splitting (E_{Rc}) in meV, momentum o□set (k_{Rc}), and the Rashba parameters in eVÅ.

Material	Space group	ICSD	K_c	E_{Rc}	k_{Rc}	a_{Rc}
PbS	186	183255	M	9.8	0.013	1.511
Bi_2O_3	159	183150	G	4.8	0.014	0.707
BrF_3	36	39441	G	12.2	0.04	0.612
O_2Se	26	99464	G	4.6	0.015	0.597
O_5Ta_2	5	280397	N	7.5	0.028	0.53
BrF_5	36	31690	G	30.6	0.127	0.484
CdP_2	33	42732	Z	3.4	0.016	0.423
AsF_3	33	35132	S	6.2	0.029	0.422
O_2Ti	35	97008	T	2.8	0.018	0.318
O_5Te_2	4	2523	Y	9.9	0.071	0.28
I_3P	173	311	K	5.3	0.093	0.115
AuCN	183	85782	L	16.7	0.025	1.353
Br_6Pb_4Se	44	21039	Z	17.5	0.03	1.159
$O_8Se_2Te_2$	1	201413	L	25.5	0.05	1.032
BrHgI	36	109010	G	11	0.022	1
Bi_2O_5Si	36	30995	G	76.2	0.157	0.97
Cl_2O_6Pb	43	40286	Z	71.1	0.152	0.937
$K_4O_3Sb_2$	186	280170	G	7.7	0.017	0.912

Ag_3S_3Sb	161	181518	F	6.4	0.014	0.892
Ag_3S_3Sb	161	605709	F	6.4	0.014	0.889
O_7STe_2	31	90837	Y	7.7	0.018	0.864
LiO_3Ta	161	84226	G	6.8	0.017	0.79
$P_2S_6Sn_2$	7	25357	G	6.2	0.016	0.766
LiO_3Ta	161	164259	G	6.6	0.017	0.759
HfO_3Sr	99	161594	G	7.2	0.019	0.743
Ga_2S_2Te	109	8028	G	5.9	0.017	0.703
AsS_3Tl_3	160	100292	Z	7.1	0.02	0.699
Cu_2S_3Sn	9	107606	G	12.3	0.041	0.597
Ag_2S_3Te	9	85135	G	6.3	0.023	0.562
$C_6O_8Tl_4$	5	260372	N	10.6	0.04	0.527
CIN	160	77911	F	17.3	0.068	0.509
P_4RuSi_4	1	79006	Z	5.2	0.021	0.494
BrO_3Tl	160	76966	Z	3.4	0.014	0.486
Al_2O_4Pb	40	80128	S	4.4	0.019	0.465
$As_5Cs_3O_9$	157	413151	A	2.7	0.012	0.443
F_2OSe	29	12110	G	5.9	0.028	0.428
$LiNbO_3$	161	28299	G	3.5	0.017	0.406
$LiNbO_3$	161	94493	G	3.5	0.017	0.406
AsC_3N_3	5	18199	G	21.3	0.105	0.405
Li_7O_6Ta	146	74950	F	7.6	0.039	0.389
Br_2O_6Sr	9	61158	X	19.3	0.106	0.365
FeP_4Si_4	1	79005	Y	2.5	0.014	0.346
$AsCoS$	29	41758	G	4.9	0.029	0.341
Cl_4NRe	79	419181	G	4.3	0.026	0.335
P_2PtSi_3	1	84944	G	4.5	0.028	0.325
AsS_3Tl_3	160	611332	Z	2	0.016	0.25
$BaBr_2O_6$	43	40287	Y	10.2	0.091	0.224
HfP_2S_6	43	47228	G	1.8	0.018	0.211
RbS_2Sb	1	200263	R	1.9	0.02	0.194
Ge_4O_9Pb	5	201282	G	11.2	0.209	0.107

Bi_2O_6TiZn	99	186801	G	18.6	0.03	1.243
Bi_2O_6TiZn	99	162766	G	18.2	0.03	1.21
$Bi_3NaO_{10}V_2$	1	88455	Z	73.3	0.142	1.035
Bi_2O_6TiZn	99	162767	Z	11	0.021	1.022
Ag_2KSe_4Ta	40	412477	S	11.6	0.029	0.791
AlBaHSi	156	162869	M	4.7	0.012	0.758
$F_3O_4PSn_3$	146	37133	F	5.2	0.015	0.674
BiP_2S_6Tl	4	249461	Y	95.9	0.34	0.564
HIO_4Zn	9	185598	G	15.4	0.056	0.556
$ClCu_3S_3Te$	160	85789	G	5.4	0.02	0.544
Cu_2RbS_4V	40	280516	Z	4.2	0.022	0.388
$CaNO_2Ta$	26	161824	G	3.8	0.02	0.371
HO_3PSn	9	25034	M	41	0.243	0.337
$AsBiCa_2O_6$	36	91475	S	9.6	0.058	0.331
$LiMo_3O_8Sc$	156	28525	G	1.4	0.019	0.151
$Bi_2O_{10}Pb_2V_2$	1	60577	G	3.3	0.048	0.14
$LiMoO_4Rb$	1	20641	G	8.8	0.324	0.054

Table S3 - Weak Rashba materials with spin splitting in the VBM. For each compound we present the ICSD code, space group, high symmetry *k*-point for the Rashba splitting in the valence band (K_v

Ag_5S_4Sb	36	16987	G	12.9	0.063	0.408
NaPSn	186	409010	G	25.2	0.136	0.372
Li_5N_2Na	6	92314	X	37	0.221	0.334
$AsLiSe_2$	9	248116	M	2.5	0.02	0.25
HgO_4S	7	28402	D	4.5	0.036	0.249
HgO_4S	31	31870	T	5.6	0.048	0.23
BaF_4Zn	36	402926	R	1.6	0.014	0.227
As_2Ba_2Cd	36	422941	G	1	0.009	0.225
$La_4O_4Se_3$	38	419128	Z	3.1	0.028	0.224
$Cl_{11}N_3P_4$	146	71913	L	24.6	0.228	0.216
O_3PbTi	99	55059	X	2.2	0.02	0.214
BaF_4Mg	36	50227	R	2.8	0.027	0.203
O_3PbTi	99	93553	X	2	0.02	0.199
Br_4OW	79	49547	X	9.2	0.093	0.197
HgO_4Se	31	412403	U	10.5	0.109	0.193
AsO_4Tl_3	4	407561	M	7.2	0.083	0.174
FH_4N	186	14294	M	9.2	0.132	0.139
K_3SbSe_4	161	65142	G	1	0.017	0.123
CO_4Rb_4	8	245438	I	4.5	0.078	0.117
Cu_2GeS_3	9	85138	G	2	0.034	0.115
I_7Nb_3Te	156	86724	G	1.8	0.032	0.114
CO_4Rb_4	8	245436	I	3.6	0.063	0.113
Li_7O_6Sb	146	15631	Z	10.4	0.246	0.085
BiO_3Sc	9	171385	N	3.3	0.08	0.082
CK_4O_4T						

$CrLiO_4Rb$	173	72552	A	37.8	0.147	0.513
$KLiO_4S$	173	86284	A	27.9	0.128	0.437
$KLiO_4S$	173	56106	A	24	0.119	0.405
$AsBrHg_3S_4$	186	280330	M	23.6	0.135	0.35
Ag_2HgI_2S	36	413300	G	5.9	0.034	0.345
H_2KO_3PS	8	75217	Z	30.9	0.212	0.291
$BaCdSb_2Yb$	36	422280	G	1.2	0.009	0.279
$Cl_4Hg_3S_2Zn$	4	420783	Z	3.5	0.025	0.276
H_3ILiN	4	55064	A	2.2	0.017	0.261
BeF_4KLi	173	2773	A	12	0.101	0.237
$AlHSiSr$	156	162868	A	2.6	0.022	0.235
CFH_6N	160	110656	L	18.1	0.222	0.163
H_2O_4PRb	43	69318	Y	4.7	0.06	0.158
$KLaSe_4Si$	4	603185	Y	2.2	0.03	0.151
$BClF_4O_2$	9	60080	Z	1.9	0.025	0.15
$Ge_2Hg_3K_2S_8$	5	281506	Y	1.2	0.017	0.148
$AsClHg_3S_4$	186	280329	M	5.9	0.086	0.136
$B_6BrK_3O_{10}$	160	172400	G	4.5	0.079	0.115
CdN_3O_6Rb	146	95537	G	1.4	0.025	0.115
$CaGaGeH$	156	173567	A	1.2	0.022	0.103
$CdKN_3O_6$	146	95538	G	O		

O

The Rashba Scale: Emergence of Band Anti-Crossing as a Design Principle for Materials with Large Rashba coefficient

1 Details of materials screening

Based on high-throughput DFT calculation, we create a large list of weak and Rashba compounds. Calculation were performed for Rashba materials candidates distilled from a list of fabricated materials. Here, we give details on the selection of non-cetrosymmetric non-magnetic compounds. This materials screening process requires to impose filters based on material properties, which can be divided in terms of those that

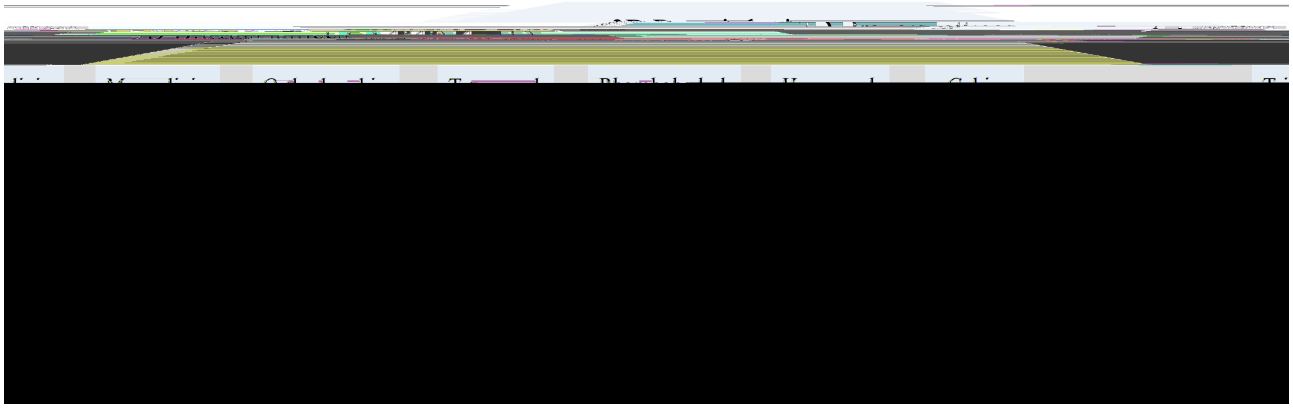

Figure S1 - Space group classification of Bravais lattices according to the inversion symmetry (IS) and asymmetry (IA); polar (P) and non-polar (NP); and space groups that could feature only the Dresselhaus e□ect (D1) or simultaneously the Rashba and Dresselhaus e□ects (RD). Here, the total electric dipole is represented by *h*, i.e., the space groups in the first line exhibit the D1 (RD) e□ect when the dipoles add up to zero (non-zero).

e□ect. In the same way, compounds with at least one polar atomic site (P), in which the atomic dipoles add up to zero, only feature the Dresselhaus e□ect. IA materials with at least one polar atomic site in which the atomic dipoles add up to non-zero can feature both Dresselhaus and Rashba e□ect. This divides the non-magnetic insulators into two groups: the first group of 5,337 consisting of NP-IA and IS compounds and the second group of 1,018 P-IA materials. The local dipoles calculation is required to identify P-IA materials in which the total dipole is non-zero. The magnitude of local dipoles depends on electron transfer, which in turns depends on the atomic species and the interaction between them. As described below, we use a strategy to infer if local dipoles add up to zero based on the atomic positions.

Total Dipole: The interatomic bondings can induce local asymmetric charge distributions. Specifically, the electron transfer in the bond between two di□erent elements creates a microscopic dipole whose direction is opposite to electron transfer direction. If all neighbor atoms were locally distributed in such a way that the dipole vectors generated by each bonding cancel each other, then the local atomic site dipole would be zero, e.g., non-polar atomic sites. This gives an intuitive way to verify if the local dipoles are zero using only geometrical information. Non-zero local dipoles can only be found in polar atomic sites, however, local dipoles can add up to zero, which can also be verified geometrically. From the 1,018 IS non-magnetic insulator with at lest one-polar site we find 867 compounds with non-zero dipole and 151 compounds in which local dipoles accidentally cancel each other. Since the electron transfer also depends on the atomic distance and

Rashba candidates. The magnitude of local dipoles depends on electron transfer, which in turns depends on the atomic species and the interaction between them.

1.3 Filters based on properties requiring orbital resolution

Rashba spin splitting: We perform high-throughput (HT) DFT calculation of the orbital-resolved band

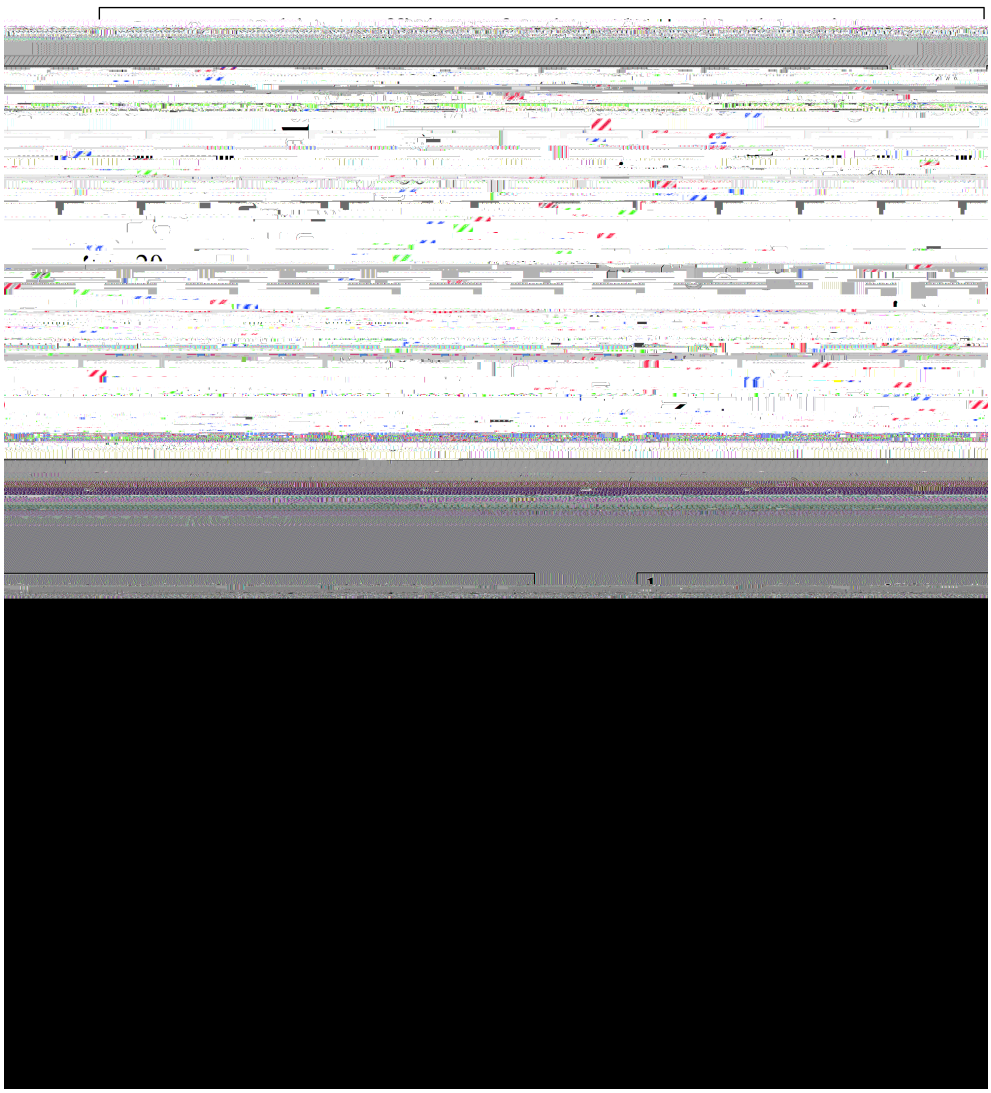

Figure S2 - DFT calculated Rashba coe□cients for the (a) valence band maximum and (b) conduction band maximum showing a general delineation (shaded blue region) into weak and strong Rashba coe□cients. The number of materials (grey bars) is defined for an interval of 0.1 eVÅ.

agreement with our previous analyses: We demonstrate in Fig. 3 (main text) that for anti-crossing bands, the smaller possible a_R is proportional to the SOC. In the one-dimensional model previously discussed, for bands without anti-crossing, $2at_{soc}$ is indeed the maximum possible a_R

The Rashba Scale: Emergence of Band Anti-Crossing as a Design Principle for Materials with Large Rashba coefficient

1 Strong Rashba materials with spin splitting in both VBM and CBM

Figure S1 - Band structure and spin texture for the compound GeTe (ICSD:659808).

Figure S2 - Band structure and spin texture for the compound PbS (ICSD:183243).

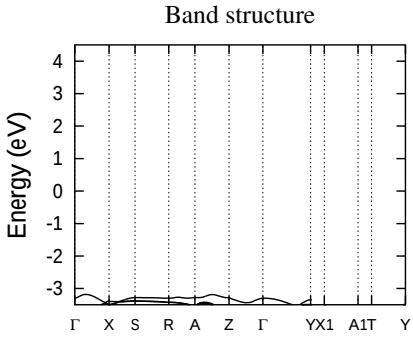

Figure S3 - Band structure and spin texture for the compound F_3Sb (ICSD:30411).

Figure S4 - Band structure and spin texture for the compound GeTe (ICSD:188458).

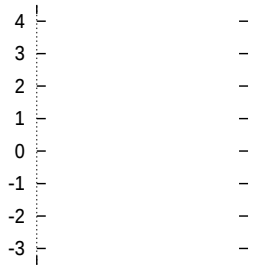

Figure S5 - Band structure and spin texture for the compound PbS (ICSD:183249).

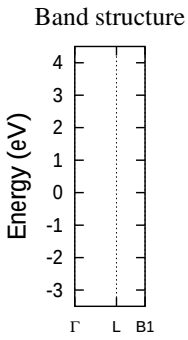

Figure S6 - Band structure and spin texture for the compound GeTe (ICSD:56040).

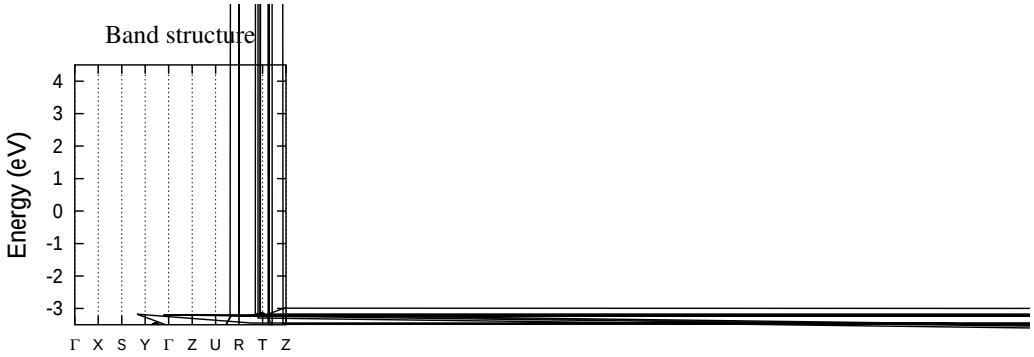
Band structure
Energy (eV)
4
3
2
1
0
-1
-2
-3
Γ X S Y Γ Z U R T Z

Figure S9 - Band structure and spin texture for the compound BiITe (ICSD:79364).

Figure S10 - Band structure and spin texture for the compound Sb_2Se_2Te (ICSD:60963).

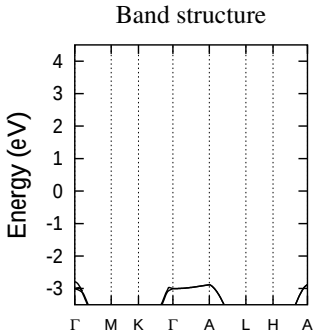

Figure S11 - Band structure and spin texture for the compound BiClTe (ICSD:79362).

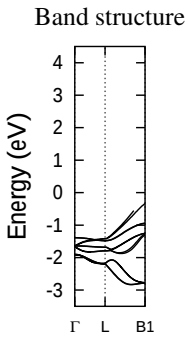

Figure S12 - Band structure and spin texture for the compound IKO_3 (ICSD:97995).

Figure S13 - Band structure and spin texture for the compound I_2O_6Zn (ICSD:54086).

Figure S14 - Band structure and spin texture for the compound Ga_2O_4Pb (ICSD:80129).

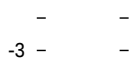

Figure S15 - Band structure and spin texture for the compound Ga_2O_4Pb (ICSD:33533).

Figure S16 - Band structure and spin texture for the compound CsF_3Pb (ICSD:93438).

-1 –
-2 –
-3 –

Figure S17 - Band structure and spin texture for the compound IKO_3 (ICSD:247719).

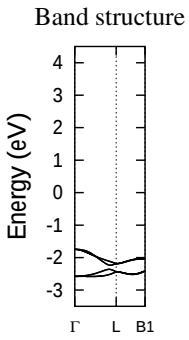

Figure S18 - Band structure and spin texture for the compound IKO_3 (ICSD:424864).

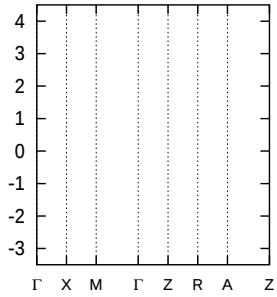

Figure S19 - Band structure and spin texture for the compound O_3PbTe (ICSD:61343).

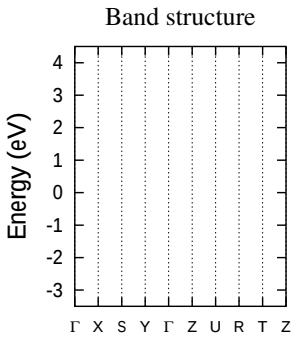

Figure S20 - Band structure and spin texture for the compound $BaCdK_2Sb_2$ (ICSD:422272).

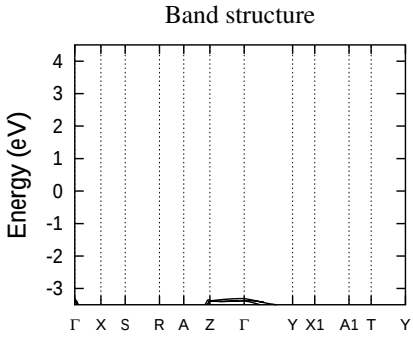

Figure S21 - Band structure and spin texture for the compound Bi_2CsCuS_4 (ICSD:93370).

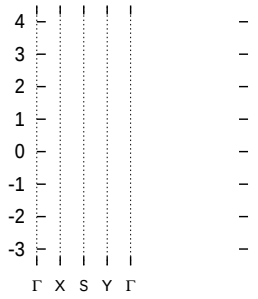

Figure S22 - Band structure and spin texture for the compound IrSSb (ICSD:74630).

2 Strong Rashba materials with spin splitting in the CBM

Figure S23: Band structure and spin texture for the compound GeTe (ICSD:659811).

Figure S24: Band structure and spin texture for the compound KSbSn (ICSD:33933).

Figure S25: Band structure and spin texture for the compound Bi_2CO_5 (ICSD:94740).

-2 –
-3 –
–
–

Figure S26: Band structure and spin texture for the compound AsKSn (ICSD:40815).

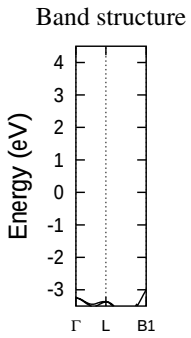

Figure S27: Band structure and spin texture for the compound IO_3Tl (ICSD:62106).

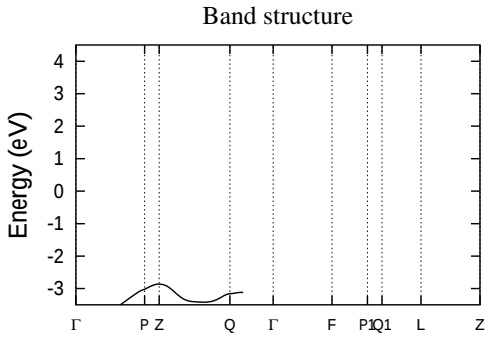

Figure S28: Band structure and spin texture for the compound S_3SbTl_3 (ICSD:603664).

-3 – –

Figure S29: Band structure and spin texture for the compound $CsGeI_3$ (ICSD:62559)150 / t0g0G0g0G1001103.4

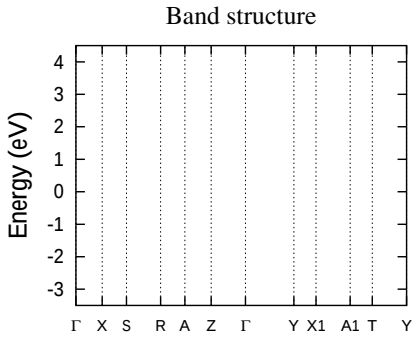

Figure S31: Band structure and spin texture for the compound Bi_2CuKS_4 (ICSD:91297).

The Rashba Scale: Emergence of Band Anti-Crossing as a Design Principle for Materials with Large Rashba coefficient

1 Strong Rashba materials with spin splitting in both VBM and CBM

Figure S1 - Band structure and spin texture for the compound GeTe (ICSD:659808).

Figure S2 - Band structure and spin texture for the compound PbS (ICSD:183243).

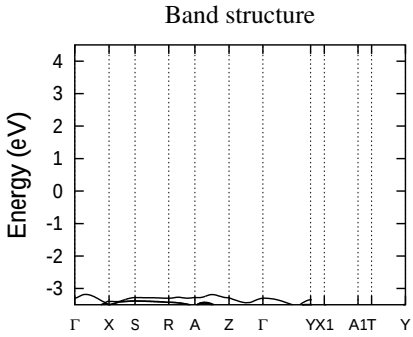

Figure S3 - Band structure and spin texture for the compound F_3Sb (ICSD:30411).

Figure S4 - Band structure and spin texture for the compound GeTe (ICSD:188458).

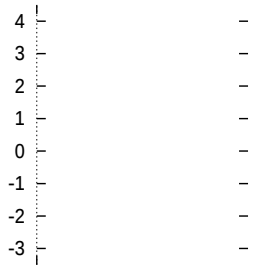

Figure S5 - Band structure and spin texture for the compound PbS (ICSD:183249).

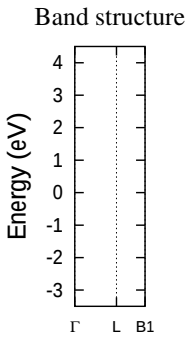

Figure S6 - Band structure and spin texture for the compound GeTe (ICSD:56040).

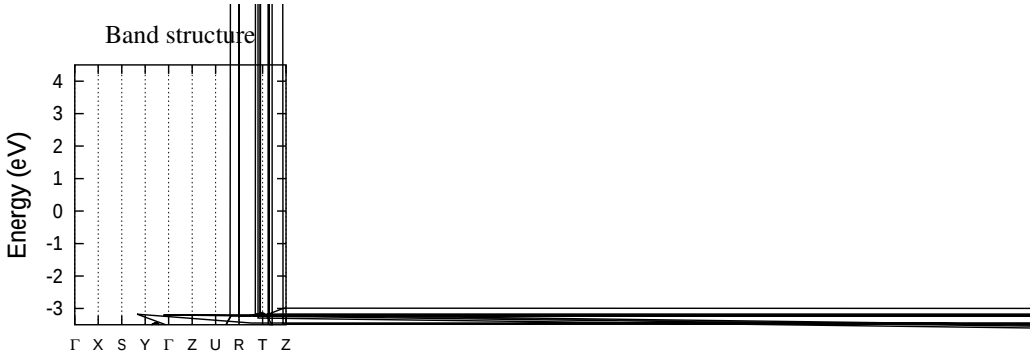
Band structure
Energy (eV)
4
3
2
1
0
-1
-2
-3
Γ X S Y Γ Z U R T Z

Figure S9 - Band structure and spin texture for the compound BiITe (ICSD:79364).

Figure S10 - Band structure and spin texture for the compound Sb_2Se_2Te (ICSD:60963).

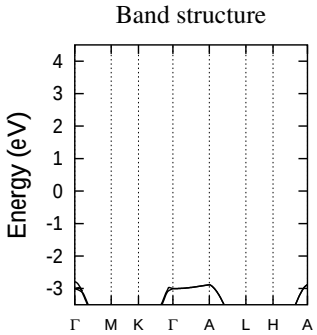

Figure S11 - Band structure and spin texture for the compound BiClTe (ICSD:79362).

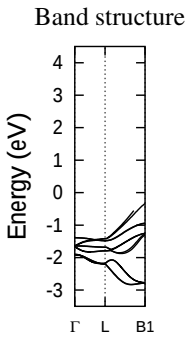

Figure S12 - Band structure and spin texture for the compound IKO_3 (ICSD:97995).

Figure S13 - Band structure and spin texture for the compound I_2O_6Zn (ICSD:54086).

Figure S14 - Band structure and spin texture for the compound Ga_2O_4Pb (ICSD:80129).

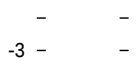

Figure S15 - Band structure and spin texture for the compound Ga_2O_4Pb (ICSD:33533).

Figure S16 - Band structure and spin texture for the compound CsF_3Pb (ICSD:93438).

-1 –
-2 –
-3 –

Figure S17 - Band structure and spin texture for the compound IKO_3 (ICSD:247719).

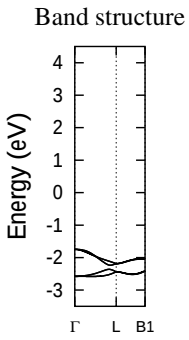

Figure S18 - Band structure and spin texture for the compound IKO_3 (ICSD:424864).

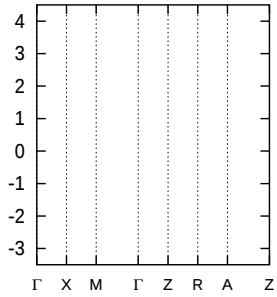

Figure S19 - Band structure and spin texture for the compound O_3PbTe (ICSD:61343).

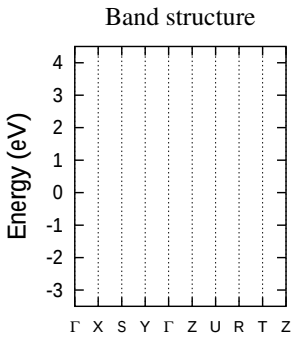

Figure S20 - Band structure and spin texture for the compound $BaCdK_2Sb_2$ (ICSD:422272).

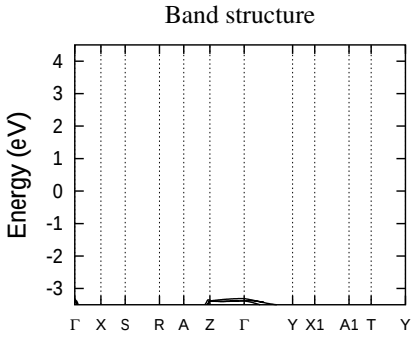

Figure S21 - Band structure and spin texture for the compound Bi_2CsCuS_4 (ICSD:93370).

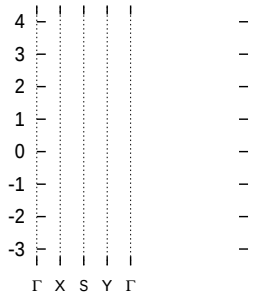

Figure S22 - Band structure and spin texture for the compound IrSSb (ICSD:74630).